PIER Letters

(Received 25 June 2024, Accepted 30 August 2024, Scheduled 30 September 2024)

Near-Field Shaping with Arbitrary Patterns and Poarization by Conformal Tensor Impedance Modulated Holographic Metasurfaces

Huifen Huang* and Ziyi Xiang

School of Electronic and Information Engineering, South China University of Technology, Guangzhou, China

ABSTRACT: Arbitrarily shaped near field with arbitrary polarization is practical application requirements. Our previous work proposed combining the phase conjugation (PC) and planar tensor impedance modulated holographic metasurface (TIMHMS) for arbitrarily shaped near field with arbitrary polarization. This paper proposes to generate arbitrarily shaped near field with arbitrary polarization by cylindrical conformal TIMHMS based on PC and Blackman window function. For the first time to the knowledge of the authors, arbitrarily shaped near field with arbitrary polarization is generated by conformal TIMHMSs. As an example, two cylindrical conformal TIMHMSs are constructed at 30 GHz for rectangle-shaped near field: (LHCP, $z = 100$ mm) and (LP, $z = 200$ mm), where LHCP and LP are left hand circular and linear polarizations, respectively. Blackman window function is used to optimize the cylindrical conformal TIMHMS design for optimized field pattern efficiency and low sidelobe. The calculated, simulated, and measured results agree well, and validate the proposed design method for conformal TIMHMS. The designed conformal TIMHMSs have the advantages of high pattern efficiency 42.1%, flexibly shaped field patterns and polarizations, and low sidelobe (-15 dB). The design method does not need complicated calculations and can be used in the upcoming sixth-generation wireless networks with required shaped near field for Radio Frequency Identification, holographic imaging, biomedical applications, etc.

1. INTRODUCTION

Conformal metasurfaces have the following advantages: being readily mounted on external surfaces to satisfy aerodynamic requirements, wide-angle scan capability, wide angle coverage, space-saving, and large-sized antenna apertures due to their 2-D structure. Conformal metasurfaces are widely used in missiles, unmanned aerial vehicles [1], and high-speed vehicles, and are candidates for communication systems and multifunction radars due to beam-scanning capabilities [2].

TIMHMS can simultaneously regulate polarization, frequency, and beam type, and has high aperture efficiency and powerful multi-function capabilities [3]. In addition, TIMHMS is fed from inside or edge of the metasurface, has low profile and easy conformation. Therefore recently, TIMHMS attracts considerable attention, and some works with good performance have been developed [4].

The spatial resolution and information capacity in the near fields are higher than that of the far fields. Several applications of such properties can be used as near-field scanning optical microscopy, evanescent near fields for super resolution, non-invasive microwave hyperthermia, Radio Frequency Identification (RFID), through-the wall imaging [5], wireless communications, detection, imaging, heating, breeding, therapy, and lithography, and many others. More signal routing and lower transmission loss can be readily achieved in the Fresnel region than the far-field region. In millimeter-Wave (mm Wave) and Terahertz (THz) frequency bands, the near-field (Fresnel) distance can amount to several dozens of meters. The near-field (Fresnel) distance is determined by D and λ. At 6 GHz and 60 GHz in the millimeter wave range, for arrays with a size of 0.1 m, the near-field distance is less than 0.5 m and 5 m, respectively. However, at 0.6 THz, the near-field distance is about 40 m. So near field may become an indispensable or even desired choice in support of simultaneous wireless power, super-high-speed data transmission, and sensing operations within a near-field region in the upcoming sixth generation (6G) mobile wireless communications networks [6]. A common key point in the applications of near fields is the generation of special field distributions. Some field shaping methods have been applied to achieve various field patterns, such as time-reversal (TR) [7]. TR method can flexibly control electromagnetic (EM) waves to generate arbitrarily shaped fields in a closed metal cavity. The extended maximum power transmission efficiency method is used to generate square-shaped, circle-shaped, triangle-shaped, and heart-shaped near-field patterns [8, 9]. However, the above techniques cannot produce shaped near field with arbitrary polarization. To the knowledge of the authors, there is no shaped near field generated by conformal metasurface. This paper researches to generate arbitrarily shaped near field with arbitrary polarization by conformal TIMHMSs based on the PC and Blackman window function. The structure of the paper is as follows. Section 2 describes the design principle. Section 3 describes the cylindrical conformal TIMHMS design. Section 4

* Corresponding author: Huifen Huang (huanghf@scut.edu.cn).

presents the simulation and measurement results, and Section 5 presents the conclusion.

2. DESIGN PRINCIPLE

Figure 1 shows a schematic of the rectangle-shaped near field by the cylindrical conformal TIMHMS. The origin of the coordinate system is at the TIMHMS center, and the X-axis is the center axis of the cylinder with radius ρ. A monopole feeder is located at the center of the TIMHMS. The operation frequency is 30 GHz, and the rectangle-shaped near field is in xoy plane.

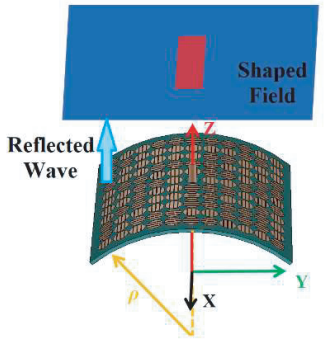

FIGURE 1. Diagram for the rectangular-shaped near-field by the conformal TIMHMS.

2.1. Phase Conjugation Technique

The electric field E of the electromagnetic wave in the passive area satisfies the vector wave equation. If the mathematical TR processing from t to $-t$ is carried out on the electric field E, the electric field E still satisfies the wave equation [10]. TR has the property of spatiotemporal focusing. When the signal is reversed between time $-T$ and 0 and sent back, the signal backtracks on the initial position and time. TR technique is operated in the time domain and is equivalent to PC operated in the frequency domain. The detail for designing the TIMHMS based on PC is in [11].

(1) First, computer holography technology is used to establish the test shaped near field through MATLAB program. Arbitrary polarization is achieved by combining x and y polarizations with related phase conditions. For instance, phase difference (90°) between the X- and Y-polarized E-fields matrix can yield circular polarization. Establishing a matrix formula corresponding to the geometry pattern of the shaped near field, arbitrarily shaped near field can be generated by MATLAB program. Then, arbitrarily shaped near field with arbitrary polarization can be obtained by MATLAB.

(2) Second, the electric field file created in MATLAB is imported into an electromagnetic simulation software (such as CST Microwave Studio) as the test field for PC operation. A geometric recording surface (with the same curvature, size, and position as the designed conformal TIMHMS) is established, and then record the received test complex-valued E-field at each grid point on the geometric surface.

(3) Third, the recorded E-field is then exported, and PC operation is performed.

(4) Fourth, the E-field performed PC operation is used for designing the conformal TIMHMS.

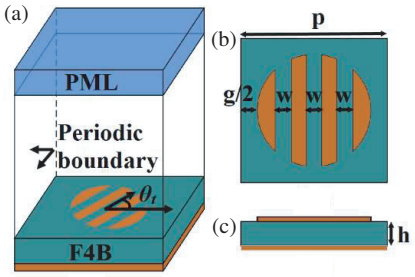

FIGURE 2. The unit cell: (a) diagram, (b) top view and (c) side view.

2.2. Surface Impedance Distribution Principle in TIMHMS

Figures 2(a)–(c) illustrate the detailed structure of the proposed unit cell, and all geometrical parameters of the cell are marked. The tensor impedance Z of the unit cell at (x, y, z) results from the interaction between the excitation surface current $\overrightarrow{J}_{surf}$ and the object wave $\overrightarrow{E}_{rad}$ [12]:

$$\bar{\bar{Z}} = \begin{pmatrix} Z_{xx} & Z_{yx} \\ Z_{xy} & Z_{yy} \end{pmatrix} = j\left[X + \frac{M'}{2}\left(\overrightarrow{E}_{rad} \otimes \overrightarrow{J^{+}}_{surf} - \overrightarrow{J}_{surf} \otimes \overrightarrow{E^{+}}_{rad}\right)\right] \quad (1)$$

where "$\otimes$" and "$+$" represent the vector inner product and Hermitian conjugate, respectively. $X = (Z_{\max} + Z_{\min})/2$ and $M = (Z_{\max} - Z_{\min})/2$. X and M represent the average impedance and impedance modulation depth, respectively. Here $X = 107.5\,\Omega$ and $M = 32\,\Omega$. A modulation depth M with window function distribution is used for optimized energy distribution on the conformal impedance surface [13]. In this paper, a modulation depth M' with Blackman window function distribution is used to optimize the pattern efficiency and minimize the sidelobe:

$$M' = M\begin{pmatrix} 0.42 - 0.5\cos\left(\frac{\pi r_{mn}}{\max(r_{mn})}\right) \\ +0.08\cos\left(\frac{\pi r_{mn}}{\max(r_{mn})}\right) \end{pmatrix} \quad (2)$$

The E-field (performed PC operation), which is arbitrarily shaped near field with arbitrary polarization, is substituted into $\overrightarrow{E}_{rad}$ matrix in Eq. (1), and any required shape can be obtained.

In the traditional TIMHMS design method, $\overrightarrow{E}_{rad}$ is directly given by the expression and is difficult to achieve arbitrarily shaped near field. The excitation surface current $\overrightarrow{J}_{surf}$ [12]:

$$\vec{J}_{surf} = \frac{(x, y, 0)}{|\vec{r}_{mn}|} e^{-j\vec{k}_t\vec{r}_{mn}} \quad (3)$$

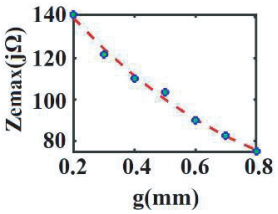

FIGURE 3. Ze versus g curve.

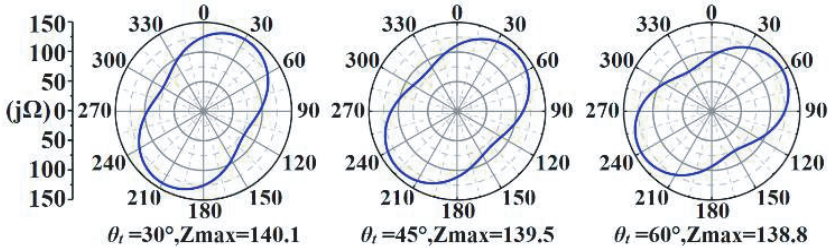

FIGURE 4. $g = 0.2$ mm, $\theta t = 30°, 45°, 60°$ equivalent scalar impedance elliptic curve.

Here, $\vec{r}_{mn}$ denotes the position coordinate vector of the unit cell in the (x, y, z) space, and the wave vector $\vec{k}_t$ in the surface wave propagation direction at angle θ_k is computed as follows [12]:

$$\begin{cases} k_t = \sqrt{k_x^2 + k_y^2} = \sqrt{\phi_x^2 + \phi_y^2}\Big/ p \\ \theta_k = \arctan\left(\frac{k_y}{k_x}\right) \end{cases} \tag{4}$$

Here, Φ_x and Φ_y represent the phase differences at the master-slave boundaries, respectively, and p is the unit cell size. Here, $(\Phi_x, \Phi_y) = (64°, 64°)$, $k_t = 658.2$. Then according to Eqs. (1)–(4), we obtain the surface impedance matrix components (Z_{xx}, Z_{xy}, Z_{yy}). The tensor impedance calculation requires large and complex accounting operations, so the effective scalar impedance k_z/k is used to simplify the unit design, which is the function of (Z_{xx}, Z_{xy}, Z_{yy}), and θ_k as follows [12]:

$$\frac{k_z}{k} = \left\{ \begin{matrix} -j(Z_0^2 - Z_{xy}^2 + Z_{xx}Z_{yy}) \\ \pm\left[\begin{matrix} -(Z_0^2 - Z_{xy}^2 + Z_{xx}Z_{yy})^2 + 4Z_0^2 \\ \times(Z_{yy}\cos^2\theta_k - Z_{xy}\sin 2\theta_k + Z_{xx}\sin^2\theta_k) \\ \times(Z_{xx}\cos^2\theta_k + Z_{xy}\sin 2\theta_k + Z_{yy}\sin^2\theta_k) \end{matrix} \right]^{1/2} \end{matrix} \right\}$$

$$\times\left[2Z_0\left(Z_{yy}\cos^2\theta_k - Z_{xy}\sin 2\theta_k + Z_{xx}\sin^2\theta_k\right)\right]^{-1} \tag{5}$$

where k_z is the wave vector in the z direction, and $k = 2\pi/\lambda$, where λ is the wavelength. The relationship of k_z/k vs θ_k is an elliptic curve. The major axis of the elliptic curve is the optimal impedance matching value $(k_z/k)_{\max}$, and the major principal axis angle $\theta_{k\max}$ is the maximum surface current direction, that is, the slot angle $\theta_t = \theta_{k\max}$.

3. THIMS DESIGN

Two cylindrical conformal TIMHMSs are designed to validate generating arbitrarily shaped near-field patterns with arbitrary polarization by conformal TIMHMS based on PC and Blackman window function techniques: (1) A left hand circular polarization (LHCP) rectangle-shaped near field with size 32 mm × 16 mm at $z = 100$ mm. (2) A y-polarized rectangle-shaped near field with size 36 mm × 16 mm at $z = 200$ mm. The proposed cylindrical conformal TIMHMS shown in Fig. 1 is formed by the unit cells in Fig. 2.

3.1. Unit Cell Design

The tensor unit cell in Fig. 2 is designed to implement the effective scalar impedance $(k_z/k)_{\max}$ calculated by (5) at (x, y, z) for the desired rectangle-shaped near field. All geometry parameters are kept fixed except for the geometry parameters g and θ_t (marked in Fig. 2) to simplify unit design. The unit cell is composed of three parts: the upper layer is a circular metal patch with three slits; the middle layer is an F4B substrate with dielectric constant 2.65; and the bottom layer is a metal ground floor. The rotation angle of the three slits of the unit cell is θ_t, and the distance between the circular metal patch and the edge of the unit cell is $g/2$. $w = 0.1$ mm, $h = 0.5$ mm, and the size of the unit cell $p = 2.4$ mm.

The relationship of the equivalent impedance vs the unit geometry parameters is as follows [12]:

$$Z_e = jZ_0\left(\frac{k_z}{k_0}\right)_{\max} = jZ_0\sqrt{1 - \frac{(\phi_x + \phi_y)^2 c^2}{4p^2\omega^2}} \tag{6}$$

where Z_0 is the impedance in free space, c the light speed in free space, and ω the angular frequency. When g varies from 0.2 mm to 0.8 mm, the surface impedance Z_e ranges from 75.5 Ω to 139.5 Ω, as depicted in Fig. 3. According to Fig. 3, a polynomial formula describing the relationship between g and Z_e can be fitted as follows:

$$Z_e = -14.0266g^3 + 103.5508g^2 - 198.4446g - 175.1247 \tag{7}$$

Figure 4 shows the curves of effective scalar impedance k_z/k vs θ_k for $\theta_t = 30°$, 45°, and 60° at $g = 0.2$ mm. Fig. 4 indicates: (1) The the long axis angle $\theta_{k\max}$ is similar to the slot direction θ_t. (2) θ_t has a minimal impact on $(k_z/k)_{\max}$, which ranges 138.8 Ω ∼ 140.1 Ω. So Z_e is mainly determined by geometry parameter g. The simulated results in Fig. 4 agree with [12].

3.2. Cylindrical Conformal TIMHMS Design

Two cylindrical conformal THIMSs formed by 31 × 31 unit cells with size 74.4 mm × 74.4 mm × 0.5 mm and conformal curvature radius $\rho = 75$ mm are designed for the rectangle-shaped near field shown in Fig. 1. Figs. 5(a1) and (a2) are the rectangle-shaped fields for (LHCP, size 32 mm × 16 mm, $z = 100$ mm) and (y-polarized, size 36 mm × 16 mm, $z = 200$ mm), respectively. The shaped fields, surface impedance, and geometry parameters (g, θ_t) distributions obtained by MATLAB are in Fig. 5. Figs. 5(b1), (c1), (d1) are the surface impedance and geometry parameters (g, θt) distributions for the LHCP field, respectively. Figs. 5(b2), (c2), (d2) are the surface impedance and geometry parameters (g, θt) distributions for y-polarized field, respectively.

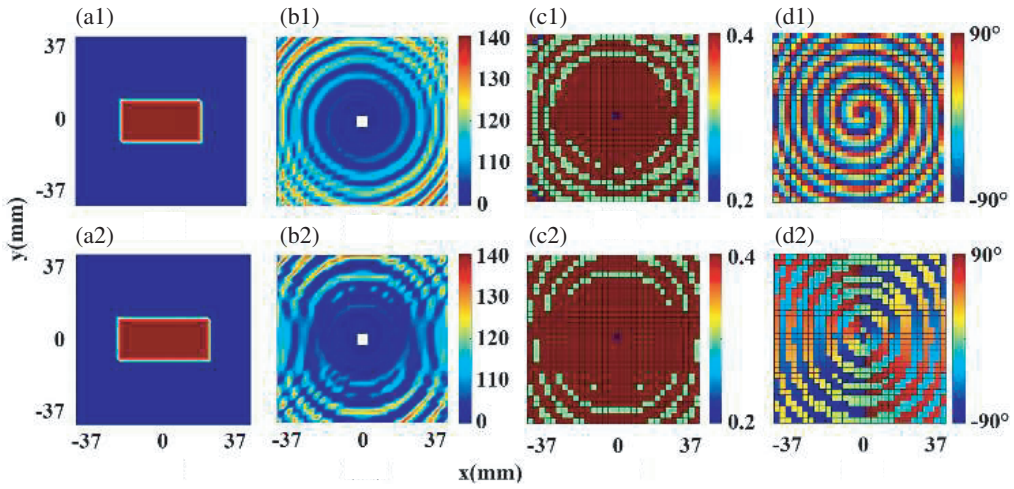

FIGURE 5. (a) The rectangle-shaped fields, (b) the surface impedance distributions, and (c), (d) geometry parameters $(g, \theta t)$ distributions. (a1)–(d1) for LHCP, (a2)–(d2) for y-polarized.

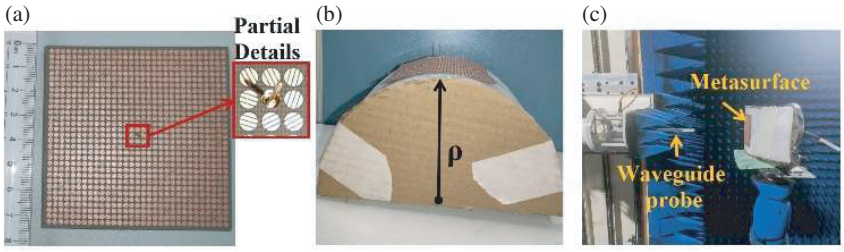

FIGURE 6. (a) Prototype and detail drawing, (b) prototype arrangement, (c) measurement environment.

4. SIMULATED AND MEASURED RESULTS

We have fabricated a prototype for the cylindrical conformal TIMHMS (LHCP, rectangle-shaped field) to validate the design, as shown in Fig. 6. Fig. 7 shows the simulated rectangle-shaped E-fields generated by the designed conformal TIMHMSs: (LHCP, size 32 mm × 16 mm, $z = 100$ mm) and (y-polarized, size 36 mm × 16 mm, $z = 200$ mm). Figs. 7(a1) and (a2) are the simulated near field by MATLAB for LHCP and y-polarized E-fields, respectively. Fig. 7(b1)/(c1) is the simulated LHCP shaped field pattern by CST with/without Blackman window function optimization. Fig. 7(b2)/(c2) is the simulated y-polarized shaped pattern by CST with/without Blackman window function optimization. The shaped near field pattern is not beautiful by using PC technique solely, and there are some sidelobes, so PC and Blackman window function are combined for the optimized sidelobe.

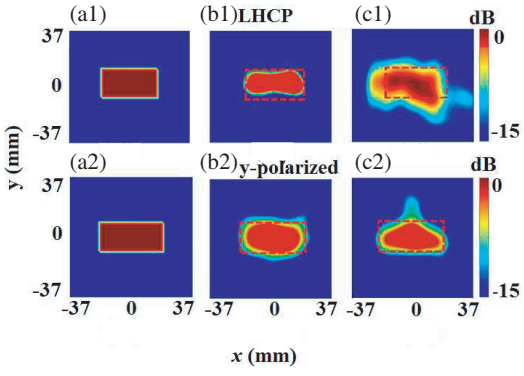

FIGURE 7. For LHCP: (a1) the generated near-field by MATLAB, (b1)/(c1) simulated shaped pattern by CST for conformal THIMS with/without Blackman window function optimization. For y-polarized: (a2) the generated near-field by MATLAB, (b2)/(c2) simulated shaped pattern by CST for conformal TIMHMS with/without Blackman window function optimization.

The simulated and measured rectange-shaped near fields (LHCP, size 32 mm × 16 mm) are shown in Fig. 8. The calculated, simulated, and measured results are in good agreement, validating the design method. The sidelobes are below −15 dB. The area for measuring the near field is 74.4 mm × 74.4 mm, and the measured position is at $z = 100$ mm.

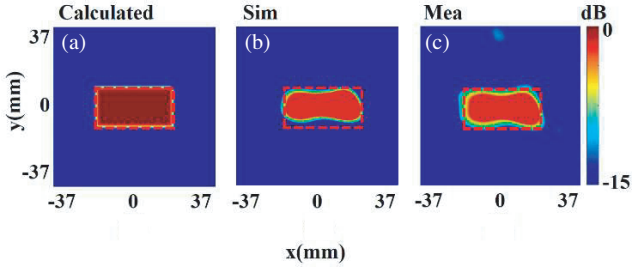

FIGURE 8. The shaped near-field for LHCP, rectangle at $z = 100$ mm: (a) generated by MATLAB, (b) simulated by CST, (c) measured.

TABLE 1. The performance of the designed conformal metasurface and near-field focusing conformal antenna in recent years.

	type	Near-field shaped field	polarization	f (GHz)	Area (λ^2)	Efficiency (%)
[11]	TIMHMS (planar)	rectangle	y-LP	18	7.44×7.44	63.3
[15]	Transmissive MS	"SEU"	LP	15	30.3×30.3	-
[16]	THIMS (conformal)	Two points	x-LP	24.125	17.13×17.13	-
[17]	array antenna (conformal)	One point	LP	2.3	3.68×3.68	-
Our work	TIMHMS (conformal)	rectangle	LHCP	30	7.44×7.44	42.1

In order to verify that the generated electric field is left-hand circularized, the E-field distributions for four phases 0°, 90°, 180°, and 270° are given as in Fig. 9. This electric field is rotated in a counterclockwise direction, and an LHCP wave is generated in the $+z$ direction.

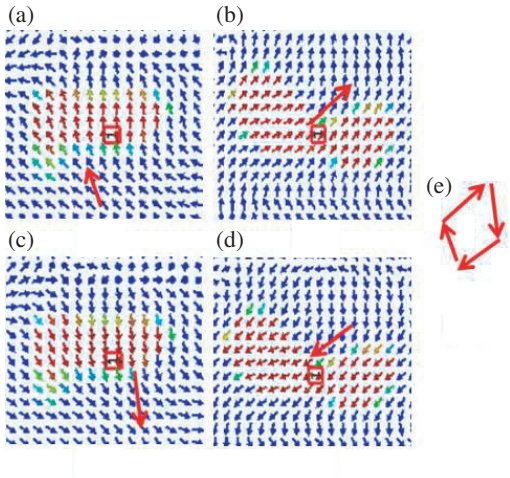

FIGURE 9. E-field distributions of rectangle-shaped near-fields are depicted as follows: (a) at 0°, (b) at 90°, (c) at 180°, and (d) at 270°.

According to [14], the ratio of P1 in the shape near-field plane to the feed transmit power P0 is the focusing efficiency, $\eta_{focus} = \frac{P_1}{P_0}$, $P_1 = \int\limits_S 1/2 \times \mathrm{Re}(\vec{E} \times \vec{H}^*) \cdot \vec{n} ds$, and the measured focusing efficiency is 42.1%, as shown in Fig. 10.

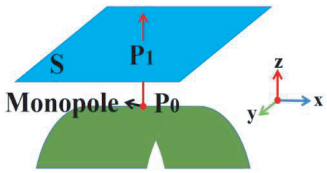

FIGURE 10. Schematic diagram illustrating the method for calculating the efficiency of shaped near-field focusing.

To indicate the advantages of our designed conformal metasurfaces, Table 1 compares the proposed design with recently published near-field shaping metasurfaces. Comparison between this paper and [11] is as follows. Similarities: Combining phase conjugation (PC) and TIMHMS is proposed by the authors, that is, the traditional formula Eq. (1) for the tensor impedance modulated holographic metasurface is also adopted. The difference between our method and conventional method in using Eq. (1) lies in the technique of obtaining the target fields ($\vec{E}_{rad}$) in (1). In this paper, $\vec{E}_{rad}$ is obtained by PC, while conventional method directly writes the expression of $\vec{E}_{rad}$. The TIMHMS designed by our method can generate arbitrarily shaped near field with arbitrary polarization. However, it is difficult for the TIMHMS by conventional method to generate arbitrarily shaped near field. Differences: This paper researches that conformal TIMHMS generates arbitrarily shaped near field with arbitrary polarization based on PC and Blackman window function being used to optimize the field pattern efficiency and low sidelobe because of a different radiation direction for each unit cell. Ref. [11] research planar TIMHMS generates arbitrarily shaped near field with arbitrary polarization based on PC. Compared with [15–17], our conformal metasurface offers several advantages: high pattern focusing efficiency, low design complexity, polarization diversity, and flexible field method. The algorithm in [15] is complex with shaped near field linear polarization and has big size. Compared with [16], our conformal TIMHMS has smaller aperture, shaped near-field pattern, while [16] is point focusing. The feed network in [17] is complex, only realizes single point focusing, and is thicker (thickness 5 mm).

5. CONCLUSION

In this paper, two cylindrical conformal TIMHMSs with a curvature radius 75 mm have been proposed, and two rectangle-shaped near fields (LHCP, size 32 mm × 16 mm, $z = 100$ mm) and (y-polarized, size 36 mm × 16 mm, $z = 200$ mm) have been generated by the two TIMHMSs, respectively. The two cylindrical conformal TIMHMSs, which can be designed to generate arbitrary field patterns with arbitrary polarizations, are designed based on PC and Blackman window function techniques. The developed cylindrical conformal THIMSs have the following advantages: for the first time to the knowledge of the authors, shaped near-field patterns are generated by conformal metasurface, flexibly shaped field patterns and polarizations, high near-field pattern efficiency 42.1%, and low sidelobe −15 dB. The calculated, simulated, and measured results are in good agreement, which verifies the design method of conformal metasurfaces with arbitrary polarization and shape near field based on PC and Blackman window function techniques.

ACKNOWLEDGEMENT

This work is supported by the Guangdong Major Project of Basic and Applied Basic Research (2023B0303000008), the National Key Research and Development Program of China (2020YFB1807300), and State Key Laboratory of Radio Frequency Heterogeneous Integration (Shenzhen University), No. 202306.

REFERENCES

[1] Williams, D. E., C. Dorn, S. Pellegrino, and A. Hajimiri, "Origami-inspired shape-changing phased array," in *2020 50th European Microwave Conference (EuMC)*, 344–347, Utrecht, Netherlands, 2021.

[2] Liang, H.-Y., H.-C. Yang, and J. Zhang, "A cylindrical conformal directional monopole antenna for borehole radar application," *IEEE Antennas and Wireless Propagation Letters*, Vol. 11, 1525–1528, 2012.

[3] Casaletti, M., M. Śmierzchalski, M. Ettorre, R. Sauleau, and N. Capet, "Polarized beams using scalar metasurfaces," *IEEE Transactions on Antennas and Propagation*, Vol. 64, No. 8, 3391–3400, 2016.

[4] Shen, Y., S. Xue, J. Yang, and S. Hu, "Tensor holographic metasurface using addition theory to independently manipulate orthogonally polarized bessel beams," *Advanced Materials Technologies*, Vol. 6, No. 4, 2001047, 2021.

[5] Catapano, I., L. Crocco, and T. Isernia, "A simple two-dimensional inversion technique for imaging homogeneous targets in stratified media," *Radio Science*, Vol. 39, No. 1, 1–14, 2004.

[6] Liu, R. and K. Wu, "Antenna array for amplitude and phase specified near-field multifocus," *IEEE Transactions on Antennas and Propagation*, Vol. 67, No. 5, 3140–3150, 2019.

[7] Zhao, D. and M. Zhu, "Generating microwave spatial fields with arbitrary patterns," *IEEE Antennas and Wireless Propagation Letters*, Vol. 15, 1739–1742, 2016.

[8] Geyi, W., "The method of maximum power transmission efficiency for the design of antenna arrays," *IEEE Open Journal of Antennas and Propagation*, Vol. 2, 412–430, 2021.

[9] Dong, Y., X. Cai, and W. Geyi, "A pattern shaping method for focused antenna arrays," *IEEE Antennas and Wireless Propagation Letters*, Vol. 23, No. 4, 1236–1240, 2024.

[10] De Rosny, J., G. Lerosey, and M. Fink, "Theory of electromagnetic time-reversal mirrors," *IEEE Transactions on Antennas and Propagation*, Vol. 58, No. 10, 3139–3149, 2010.

[11] Huang, H.-F., Z.-Y. Xiang, and J.-F. Mao, "Generating arbitrary shaped near-field with arbitrary polarization by combining tensor holographic impedance metasurface and phase conjugation techniques," *IEEE Antennas and Wireless Propagation Letters*, Vol. 23, No. 7, 1971–1975, 2024.

[12] Fong, B. H., J. S. Colburn, J. J. Ottusch, J. L. Visher, and D. F. Sievenpiper, "Scalar and tensor holographic artificial impedance surfaces," *IEEE Transactions on Antennas and Propagation*, Vol. 58, No. 10, 3212–3221, 2010.

[13] Kong, X., Y. Tian, Q. Feng, and L. Li, "High-efficiency cylindrical conformal holographic metasurface based on tensor impedance modulation surface," in *2022 IEEE MTT-S International Wireless Symposium (IWS)*, Vol. 1, 1–3, Harbin, China, 2022.

[14] Liang, Y., H. Liu, F. Wang, H. Meng, J. Guo, J. Li, and Z. Wei, "High-efficiency, near-diffraction limited, dielectric metasurface lenses based on crystalline titanium dioxide at visible wavelengths," *Nanomaterials*, Vol. 8, No. 5, 288, 2018.

[15] Wu, J. W., R. Y. Wu, X. C. Bo, L. Bao, X. J. Fu, and T. J. Cui, "Synthesis algorithm for near-field power pattern control and its experimental verification via metasurfaces," *IEEE Transactions on Antennas and Propagation*, Vol. 67, No. 2, 1073–1083, 2019.

[16] Wang, H., S. Yu, and N. Kou, "Design of cylindrical holographic impedance metasurface for near-field focusing," *Progress In Electromagnetics Research Letters*, Vol. 106, 129–134, 2022.

[17] Li, Y., S. Yu, N. Kou, Z. Ding, and Z. Zhang, "Cylindrical conformal array antenna for near field focusing," *International Journal of RF and Microwave Computer-Aided Engineering*, Vol. 32, No. 6, e23135, 2022.